

Chapter 1

X-RAY ABSORPTION FINE-STRUCTURE SPECTROSCOPY: PRINCIPLES

1.1. Simple Theory

The interaction of X-ray photons (below approximately 50 keV) and matter is dominated by photoelectric excitation processes which manifest themselves as absorption edges when the photon energy matches the binding energy of electrons in atomic core levels. The loss of X-ray intensity I with absorber thickness x defines the linear absorption coefficient $\mu(E)$ via the exponential attenuation law

$$\frac{I(E)}{I_0(E)} = e^{-\mu(E)x}, \quad (1.1)$$

where $I_0(E)$ is the X-ray intensity prior to entering the sample. The determination of $\mu(E)$ has historically been carried out by measurements of the transmission of appropriately prepared, thin samples [1-6]. Yield measurements are based on the fact that the decay of each photoelectrically formed core hole results in the emission of fluorescent photons and/or Auger electrons, the number of which being proportional to the absorption coefficient. They are nowadays standard methods for the acquisition of X-ray absorption information, but have found widespread use only since the 1970s [7-17]. Because of favourable signal-to-background characteristics, measurements of fluorescence yields have become the most important method for the study of samples containing the absorber of interest in highly diluted form [11,18-20]. Fluorescence yield detection suffers from considerable nonlinearities in its response to the X-ray absorption coefficient ('self-absorption effects') when concentrated samples are investigated [17,21-24]. The variants of electron yield (EY) detection (partial EY, total EY, Auger EY) have been used mainly for surface science applications, as the intrinsic surface sensitivity of electron detection leads to advantageous signal-to-noise characteristics. However, electron-yield detection has very recently found increasing attention also as an alternative method to transmission studies of concentrated and/or bulk samples. Its characterisation for this purpose is the object of the studies described in this thesis.

The existence of small modulations in the X-ray absorption coefficient in the vicinity of the edge and on its high-energy side, commonly termed X-ray absorption fine-structure (XAFS) has been known since the early days of fundamental research into the properties of X-rays (the history of XAFS theory has been summarised in [25]). Although it was recognised very early [25] that the structure near the edge (XANES,

X-ray absorption near-edge structure) had strong contributions due to electronic transitions to unoccupied electronic states below the continuum threshold [26-28], it was only in the early 1970s that the extended X-ray absorption fine structure (EXAFS) was explained by a theory accurate and quantitative enough to trigger the development of X-ray absorption spectroscopy (XAS) into the routinely used structural probe known today [29-34]. It was established that the EXAFS occurring at energies beyond approximately 50 eV from the edge is due to the interference between the outgoing photoelectron wave and the fraction of it which is scattered back from neighbouring atoms (figure 1.1.). This short-range theory therefore explained the EXAFS by a modulation of the final state wavefunction due to the varying electron density of the backscattered wave at its origin. It is easily shown that the Fourier transformation of the EXAFS function produces a pseudo-radial distribution function of the atoms in the close vicinity of the absorbing atom. The single scattering interpretation of the EXAFS therefore provides structural information about the short-range environment of the X-ray absorbing atoms, making the technique extremely valuable for structural studies of non-, poorly- or polycrystalline materials and biological systems [35].

The EXAFS function $c(k)$ is commonly described as the variation of $\mathbf{m}(k)$ about the smoothly varying background $\mathbf{m}_0(k)$:

$$c(k) = \frac{\mathbf{m}(k) - \mathbf{m}_0(k)}{\mathbf{m}_0(k)}. \quad (1.2)$$

A semi-phenomenological expression for $c(k)$ which contains most of the basic physics underlying the EXAFS phenomenon in the single scattering approximation has been given by Stern [25,32]. This form of the EXAFS theory was and, by some authors, still is, (see e.g. [36,37]) applied to the data analysis throughout the first decade of EXAFS studies. Because of its simplicity and conceptual value as a vehicle for subsequent discussions, this standard EXAFS equation shall be briefly derived.

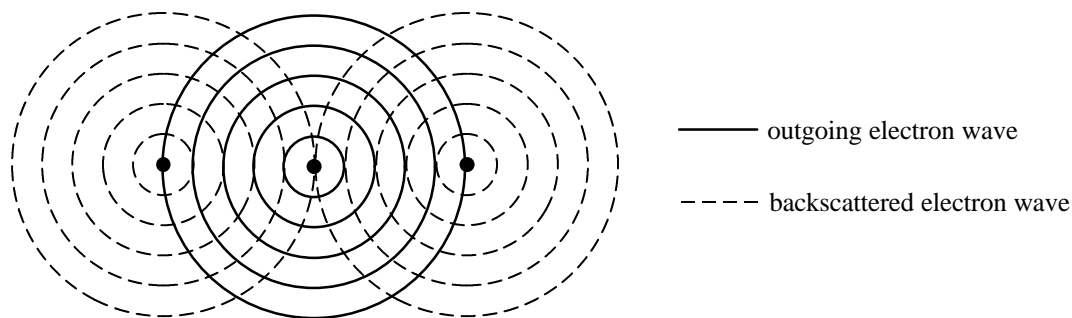


Figure 1.1. Schematic view of the radial component of the outgoing and backscattered parts of the photoemitted electron wave in a triatomic molecule excited at the centre atom. Interference between the outgoing and backscattered components leads to the modulation of the final state wavefunction in dependence on electron energy, and thus to the fine structure of the X-ray absorption coefficient.

The amplitude of a spherical photoelectron wave of wavenumber $k = 2p/l$ (where λ is the photoelectron wavelength λ) at the distance r from its origin is proportional to $r^{-1} \cdot \exp(ikr)$. The amplitude fraction which survives at the origin after backscattering from an atom at distance r_i is thus proportional to $F_i(2k) \cdot r_i^{-2} \cdot \exp(i2kr_i)$, where $F_i(2k)$ is the backscattering amplitude characteristic of the scattering atom. This expression would be adequate for an electron wave moving in a constant potential. In reality, the electron is accelerated and decelerated as it moves, respectively, in and out of the atomic potentials, resulting in a term $\mathbf{d}_i(k) - \mathbf{p} / 2$ which has to be added to the phaseshift $2kr_i$ in the expression for the backscattered amplitude. It can be shown (see equation 1.7 below) that the real part of the backscattered amplitude is proportional to the modulation of the dipole matrix element for the transition to the final state. Hence the $c_i(k)$ function induced by any neighbouring atom i becomes:

$$c_i(k) = \frac{m}{2ph^2k^2} \frac{f_i(2k)}{r_i^2} \sin[2kr_i + \mathbf{d}_i(k)]. \quad (1.3)$$

Here, $F_i(2k)$ has been replaced according to

$$F_i(2k) = \frac{m}{2ph^2k^2} \frac{f_i(2k)}{K}, \quad (1.4)$$

where K is a proportionality constant.

The photoemission event is a many-body process, *i.e.*, the photoelectron interacts with other electrons in the excited atom from which it originates, through so-called intrinsic inelastic processes, and with electrons it encounters along its path to and back from the scatterer (in extrinsic loss events). Intrinsic processes include the effects of the finite core hole life-time (interference requires coherence, *i.e.*, that the returning photoelectron wave encounters the same potential as the outgoing wave) as well as shake-up and shake-off processes, which involve the rearrangement or removal, respectively, of other electrons on the excited atom. The EXAFS amplitude loss due to multiple photoexcitation in shake-up processes is taken into account by a constant amplitude factor S_0^2 the theory of which is well understood [38,39].

Depending on the type of atom and core excitation involved, S_0^2 takes on values which are typically between 0.6 and 0.9. Other many-body effects can be phenomenologically approximated by a mean free path l [25], introducing an exponential decay term $\exp(-2r_i/l)$ into equation (1.3). These extensions result in an EXAFS equation of the form

$$\mathbf{c}_i(k) = \frac{m}{2ph^2k^2} S_0^2 \frac{f_i(2k)}{r_i^2} \exp\left(-\frac{2r_i}{l}\right) \sin[2kr_i + \mathbf{d}_i(k)]. \quad (1.5)$$

The experimentally determined EXAFS amplitude $\mathbf{c}(k)$ is the superposition of the EXAFS contributions $\mathbf{c}_i(k)$ from all atoms i surrounding the photoabsorber. Similar atoms ($\Delta Z \approx \pm 5$) at similar average distances $R_j \approx r_i$ ($\Delta R_j \approx \pm 0.6 \text{ \AA}$) cannot be resolved by the technique and must be treated as part of a coordination shell characterised by a coordination number N_j . Thermal vibrations and/or structural disorder give rise to small variations of the average absorber-backscatterer distance within one shell. If the disorder is small and characterised by a Gaussian distribution then it dephases the EXAFS additionally by a factor $\exp(-2k^2 \mathbf{s}_j^2)$, wherein \mathbf{s}_j^2 represents the mean-square variation in R_j . Introducing this Debye-Waller factor (the value of which is *not* identical to the Debye Waller factor obtained by X-ray diffraction techniques [40-44]) and summing over all coordination shells gives for the final single-scattering EXAFS expression:

$$\mathbf{c}(k) = \frac{m}{2ph^2k^2} \sum_i S_0^2 N_i \frac{f_i(2k)}{R_i^2} \exp(-2k^2 \mathbf{s}_i^2) \exp\left(-\frac{2R_i}{l}\right) \sin[2kR_i + \mathbf{d}_i(k)] \quad (1.6)$$

If certain assumptions are made, this simple equation can be derived from first principles [25,38], confirming that it is a physically valid approximation to the EXAFS. However, the simplifications underlying its derivation make it generally too inaccurate for meaningful EXAFS analyses based on a theoretical expression. The basic features of more advanced calculation schemes for the EXAFS analysis will now be outlined.

1.2. Improvements to the Simple Theory

Time dependent perturbation theory yields the atomic X-ray absorption cross section in the form of Fermi's Golden Rule [45] for dipole transitions as

$$\mathbf{m}(\mathbf{w}) = \frac{4\mathbf{p} \cdot e^2 \mathbf{w}}{c} \cdot |\langle f | \mathbf{e} \cdot \mathbf{r} | i \rangle|^2 \cdot \mathbf{r}(E_f), \quad (1.7)$$

where \mathbf{e} is the polarisation vector of the electric field of the X-ray beam and $\mathbf{r}(E_f)$ the density of allowed states at the final state energy E_f [38]. It is an important feature of equation (1.7) that the EXAFS is principally dependent on the orientation of the electric field vector and hence the X-ray incidence angle and/or polarisation vector with respect to the sample orientation [44,46]. This constitutes one of the most

important extensions to the simple theoretical expression (1.6), which is valid only for samples of cubic symmetry and polycrystalline/amorphous specimens.

Within the scattering approach to the description of the EXAFS amplitude the density of the allowed final states $r(E_f)$ in equation (1.7) must be that of a free electron of wavevector k and energy $\hbar^2 k^2 / 2m$. As a result, only the matrix element in equation (1.7) can give rise to the EXAFS, yielding, because the initial-state wavefunction $|i\rangle$ is fixed, the modulation of the final-state wavefunction $|f\rangle$ as the origin of the EXAFS. The energy of the outgoing photoelectron wave is given by

$$\hbar^2 k^2 / 2m = E_f - E = \hbar\omega - E_{edge} + E_0, \quad (1.8)$$

where E is the energy of a free electron of zero wavevector in the sample, which is equivalent to the effective mean potential seen by the photoelectron. The energy E_{edge} of the experimentally observed absorption edge occurs at the lowest unoccupied, allowed energy level (in conductors the Fermi energy) and is offset from the true initial binding energy of the photoelectron by E_0 , the so-called threshold energy. The threshold energy is sample specific and difficult to derive from first principles. It is therefore included as a fitting parameter in the data analysis. Note that it is always negative, typically of the order of -10 eV [38].

Eq. (1.7) is the starting point for the derivation of any rigorous theoretical expression for the EXAFS function. The space constraints do not allow a thorough discussion of *ab initio* EXAFS calculation schemes which have been obtained over the last two decades (see, e.g., [25,38,47-54]). The reader is referred to an excellent summary of the present state-of-the-art given in the thesis of Newville which is, at the time of writing, readily available on the *world-wide web* [55]. The final expressions for the EXAFS are similar to equation (1.6), but the individual terms in it (phase shifts, backscattering amplitudes, many body losses, static and thermal disorder) reflect the more complex nature of the underlying physical processes. The most fundamental additional features account for curved wave effects and the influence of multiple scattering. Both additions shall be introduced briefly.

The heuristic derivation outlined in section 1.1 was implicitly based on the assumption that the spherical photoelectron wave could be approximated by a plane wave incident on the backscattering atom. This so-called ‘small atom approximation’ is only valid if the effective size of the backscattering atom is small compared to its distance to the photoelectron origin [56]. For low values of k this is generally not the case, as the low-energy photoelectron wave is backscattered at outer atomic shells. For large values of k the small-atom approximation becomes a somewhat better representation of the scattering process because higher-energy electrons penetrate the

atomic core deeper before scattering. Note, however, that the accuracy of the small-atom approximation is principally unsatisfactory for a fully theoretical EXAFS analysis, even in the high- k region [38]. The rigorous EXAFS theory which takes the curvature of the photoelectron wave accurately into account is well known [46]. However, it is rarely adopted for practical analysis purposes because of the substantial computational effort involved in its evaluation. A simplified exact version of the rigorous theory can be derived for polycrystalline and amorphous samples [38,53,54]. This approach is known as the fast curved-wave (FCW) theory and speeds up EXAFS calculations sufficiently to be applicable in quick data fitting routines. It is the form of the EXAFS theory which has been employed for the data analysis in the present work [53,54,57].

The single scattering approximation, also implicit in the derivation of equation (1.6) [25,38], assumes that the backscattered photoelectron wave undergoes only one scattering event before interfering with the outgoing wave at the origin. With the exception of diatomic molecules, this approximation is principally not valid because there is always a finite probability that the outgoing electron wave is scattered back along a multiple scattering path (see fig. 1.2). A well-known example for pronounced multiple scattering is the forward focusing effect in lattices of fcc- [48] and NaCl-symmetry [58], where the six nearest neighbours are collinearly aligned with six atoms from the fourth coordination shell. Forward scattering through the middle atom enhances the backscattering contributions from the fourth shell [48,49,58,59]. In summary, the single scattering theory is usually a good approximation for the interpretation of nearest neighbour EXAFS contributions, while multiple scattering becomes important for the interpretation of the EXAFS contributions from higher coordination shells, especially in the presence of low- Z atoms, as, e.g., in oxides. It should be noted that the computational effort required for a full multiple scattering analysis of the XAFS is potentially enormous. Approximate, fast schemes have been developed, however, the most valuable of them being currently the GNXAS [51,52] and FEFF curved-wave *ab-initio* codes [48-50,59-61]. The recent FEFF codes (version 5 and 6) have been used in the present study to identify multiple scattering

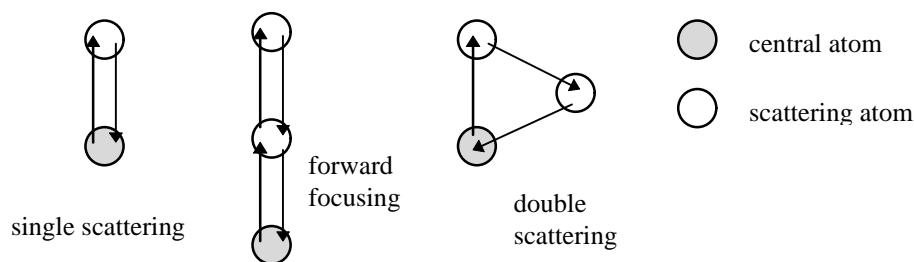


Figure 1.2. Examples for simple multiple scattering paths.

effects. The FCW theory employed for the EXAFS fitting analysis does likewise include an option for the evaluation of some higher order scattering terms [53], but little use was made of this feature.

Further improvements to the simple theory include more advanced treatments of the inelastic losses in many-body interactions [38,48,49,62], particularly of static disorder [63,64] and thermal motion [40,65-68]. However, most of these features will not be necessary to use here. An exception is the k -dependence of the mean free path $I(k)$ for extrinsic losses which is included in the analysis code as described in [38]. Finally, after taking curved-wave, multiple scattering and many body effects into account, the theoretical expression for the EXAFS is best expressed as a sum over all possible scattering paths Γ of length R , hence (here in Hartree atomic units with $e = m = \hbar = 1$)[48]

$$\mathbf{c}^{\Gamma}(k) = \sum_{\Gamma} \frac{S_0^2}{kR^2} |f_{eff}^{\Gamma}(k)| \exp\left(-\frac{2R}{I(k)}\right) \exp\left(-\frac{2S_{\Gamma}^2}{k^2}\right) \sin[2kR + \mathbf{f}_{\Gamma}(k) + 2\mathbf{d}_c(k)] \quad (1.9)$$

where f_{eff}^{Γ} is the effective curved-wave scattering amplitude for each path Γ , $\mathbf{f}_{\Gamma}(k)$ is the effective phase shift of the scattering path, $\mathbf{d}_c(k)$ is the final-state phase shift at the central atom, and $\exp(-2S_{\Gamma}^2/k^2)$ is the effective Debye-Waller factor for Γ .

1.3. Data Reduction and Background Subtraction

Most of the experimental data described in this study were recorded in several scans of the same spectrum rather than collecting a single, long scan. While this approach results in longer data collection times (due to the accumulation of deadtime between the acquisition of spectral datapoints) it has the advantage of identifying the presence of low frequency noise in the spectra. In general, if not stated otherwise, data were deemed acceptable only in the absence of significant deviations between single scan data from the same sample. To facilitate the treatment of a large number of data files, a data reduction program (running under the Windows operating system) has been written by the author which allows on-screen plotting of all information contained in the Daresbury Laboratory file format and subsequent storage of the processed data in two-column ASCII file format. The scope of features contained in this utility is essentially equivalent to the Daresbury Laboratory reduction program EXCALIB, with a few additions, most notably provisions for the plotting of the incident photon beam intensity. In contrast to the Daresbury Laboratory program, all data reduction steps can be performed *unattended* in an automated fashion. The program thus proves very time saving, particularly in the

analysis of the large data bodies which are obtained by time-resolved experiments with a quick scanning monochromator.

The first step of the data analysis consists in examining the experimental data for irregularities, such as spikes, glitches or other unusual features in the background function. In the most obvious cases, these can sometimes be removed by careful editing of the raw spectrum and/or interpolation between neighbouring datapoints. After completion of these preliminary analysis steps the spectral background must be removed. The analysis of the EXAFS function requires its separation from the smooth background function $\mathbf{m}_0(E)$ (as defined in equation (1.2)) which is often also referred to as the atomic absorption. It comprises the pre-edge region, the edge step and the post-edge background. Because the function $\mathbf{m}_0(E)$ is generally unknown, approximate background subtraction procedures of different degrees of sophistication have been developed in the past. Virtually all of them follow a three step process, including (i) fitting and subtraction of the pre-edge background, (ii) normalisation of the resulting spectrum, and (iii) fitting and subtraction of the post-edge background [69-72]. This approach was adopted in the present work. Note that more advanced procedures are the object of active research [73].

The pre-edge background subtraction is usually the most uncritical step in the background removal procedure, as it simply involves the fitting of a low-order polynomial (first or second order) to the experimental pre-edge data. It is sometimes recommended that the pre-edge function is fitted using Victoreen's empirical expression for the energy dependence of the X-ray absorption coefficient [70], but the error introduced by careful use of polynomials is usually negligibly small [69]. All EXAFS functions included in the present work were therefore obtained by subtracting a second order polynomial, which was extrapolated in the post-edge region to fit an appropriately chosen point at the end of the spectrum (see section 1.4). As can be seen by inspection of figs. 1.3-1.5, this 'steering' of the polynomial at the end of the spectrum compensates for sloping background functions.

Because of the uncertainties about the true background function $\mathbf{m}_0(k)$ (cf. equation 1.2) great care must be taken not to distort the EXAFS information in the process of fitting an approximate background function and normalising the spectrum. Most critical is the choice of the post-edge background function $\mathbf{m}_{bg}(k)$ because of its pronounced influence on the amplitude of the extracted EXAFS information. One common way of avoiding this problem is to normalise the pre-edge background subtracted spectrum $\mathbf{m}(k)$ to the height of the absorption edge step $\mathbf{m}(k_s)$ [69]. The EXAFS function

$$c(k) \approx \frac{\mathbf{m}(k) - \mathbf{m}_{bg}(k)}{\mathbf{m}(k_s)} \quad (1.10)$$

is then obtained. However, this procedure is inappropriate when, as in the present work, the EXAFS analysis is based on fitting theoretical parameters. Problems arise because the edge-step height is generally larger than the true post-edge background function at high energies (> 250 eV) beyond the edge. The edge step normalisation therefore reduces the amplitudes of the EXAFS at high k -values artificially, entailing erroneous fitting results for the amplitude parameters (coordination numbers and Debye-Waller factors). The fitting analysis requires that the true background is modelled by a function $\mathbf{m}_{bg}(k)$ for all values of k . In other words, the aim is to ensure that the approximation

$$c(k) = \frac{\mathbf{m}(k) - \mathbf{m}_0(k)}{\mathbf{m}_0(k)} \approx \frac{\mathbf{m}(k) - \mathbf{m}_{bg}(k)}{\mathbf{m}_{bg}(k)} \quad (1.11)$$

is fulfilled to an acceptable degree.

All background subtractions in the present work have been carried out using the relevant routines included in the commercial PAXAS program [74] rather than the much less elaborated public Daresbury Laboratory packages EXBACK and EXBROOK. The PAXAS approach to the post-edge background subtraction is essentially based on procedures set out first in the work of Cook and Sayers [72]. The principal idea consists in maximising the physically meaningful EXAFS amplitude information at the expense of low- and high-frequency noise in the data. The background subtraction is thus an iterative process of examining the extracted EXAFS information as a function of the post-edge background function parameters. This is achieved by Fourier-transforming the k^n -weighted (usually for $n = 3$) EXAFS function and dividing the resulting R-space spectrum of the Fourier-transform (FT) into three regions: low-frequency contributions ($R < \approx 1 \text{ \AA}$), high-frequency noise ($R > \approx 5 - 6 \text{ \AA}$) and the physically meaningful data range between the two. The original Cook-Sayers algorithm simply optimises the post-edge background function by integrating the Fourier transform and minimising the integral fraction in the low-frequency region [72]. The quality of the post-edge fit is thus evaluated using the criterion

$$R_2 = \frac{\int_0^{R_{low}} |FT(k^n \cdot c(k))| \cdot dR}{\int_0^{R_{max}} |FT(k^n \cdot c(k))| \cdot dR}, \quad (1.12)$$

where R_{low} is the chosen upper limit to the low-frequency range in the Fourier transform, and R_{max} the maximum evaluated R-value. This single criterion has an important drawback, namely that the n -weighting of the EXAFS spectrum (n -values of 2 or 3 are necessary to ensure that the background functions can be fitted in the high- k region) entails insensitivity to EXAFS information in the lower k -range. In PAXAS, this quality criterion is therefore complemented by the evaluation of the match between the back-transformed R-window deemed to contain the meaningful EXAFS information $c_b(k)$ and the unfiltered EXAFS function $c(k)$ according to

$$R_1 = \frac{\int_{k_{min}}^{k_{max}} |c(k) - c_b(k)| \cdot k^m \cdot dk}{\int_{k_{min}}^{k_{max}} c(k) \cdot k^m \cdot dk}, \quad (1.13)$$

where k_{min} and k_{max} denote the lower and upper limits to the evaluated k -range of the EXAFS function. The weighting factor m was chosen as 1 to ensure that EXAFS contributions from the lower k -range were represented in the evaluation of the background function. The quality of the background function was characterised by a total fit factor R , defined as

$$R = W_{R_1} \cdot R_1 + W_{R_2} \cdot R_2, \quad (1.14)$$

where the weighting factors W_{R_1} and W_{R_2} were both chosen as 0.5. It should be noted that variation of the weighting factors does not in practice introduce very pronounced differences, particularly with good-quality, noise-free EXAFS data.

All post-edge background functions were first optimised by using a cubic smoothing spline [75] to fit the post-edge background function $m_{bg}(k)$. Using a spline function for this purpose can lead to inaccurate results if residual curvature in the smoothed spline follows the EXAFS oscillations. In this case, an artificial reduction of the EXAFS amplitude information from the nearest neighbours occurs. The post-edge fit was therefore always carefully examined for the possibility of EXAFS amplitude loss and comparative post-edge background subtractions were carried out using polynomials (between 3rd to 6th order) [69]. When it was found that the polynomial resulted in better EXAFS functions (as judged by the overall amplitude information *and* by the R value given by equation (1.14)) then it was employed for the final background subtraction.

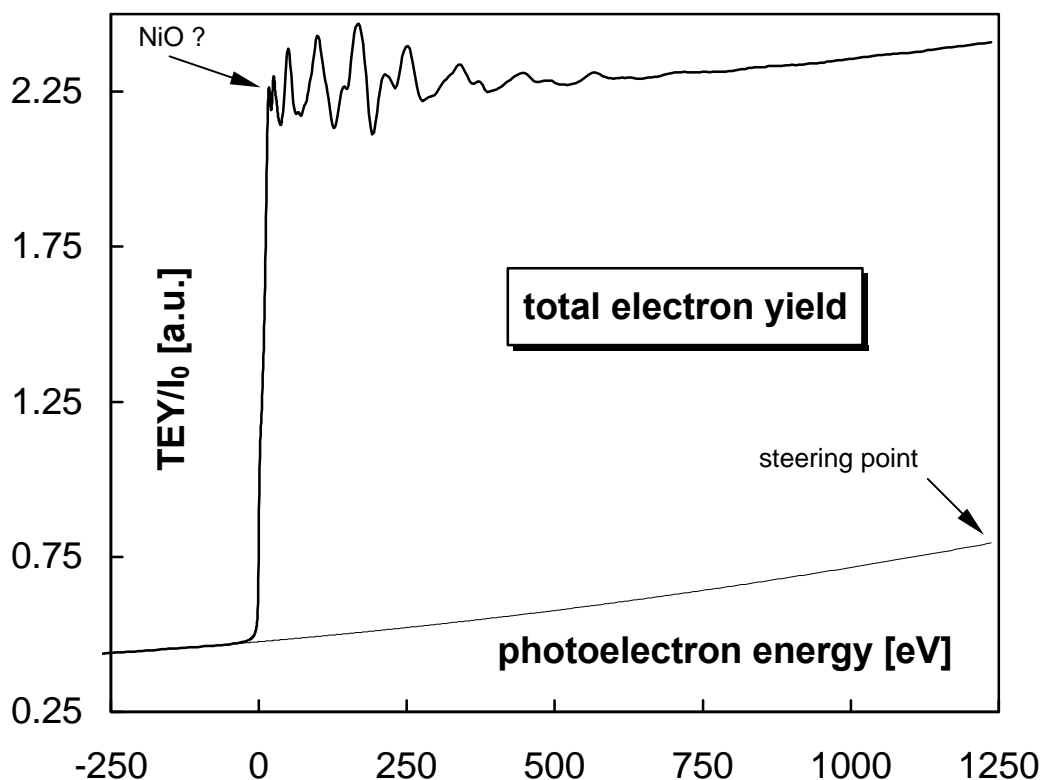


Figure 1.3. Representative electron-yield spectrum (polycrystalline Ni) with fitted 2nd-order polynomial pre-edge background function. The arrows indicate (i) a near-edge feature indicative of the presence of less than 2% of NiO contributions to the spectrum, and (ii) the position of the pre-edge ‘steering point’ used to obtain an appropriately upwards sloping pre-edge background function.

1.4. Normalisation of Total Electron-Yield EXAFS Spectra

It is expected that complications will arise with respect to the normalisation of the EXAFS data when TEY data are compared to EXAFS results obtained using other detection techniques, especially transmission configurations. This is illustrated in figures 1.3. to 1.5. which compare gas-flow TEY and transmission data obtained from metallic Ni samples*. The most notable difference between both spectra is the different sign of the slope of the background function. In the case of electron-yield detection, the background monotonically increases throughout the whole spectrum due to the increase in the flux of emitted photoelectrons and secondary electrons with X-ray energy. In contrast, the transmission background function exhibits the well-

* Both Ni K-edge (8.33 keV) datasets were acquired on the focused-beam XAFS station 8.1 of the EPSRC Daresbury Laboratory using a double-crystal Si(220) monochromator. The He-flow total electron-yield spectrum was recorded in a single scan (24 min) in November 1995, at a storage ring current of 135 mA. The single-scan transmission data (collection time: 55 min) were obtained in March 1992 with a ring current of 210 mA. The angle of X-ray beam incidence was in both cases 90° with respect to the surface plane.

known decaying Victoreen form [76-78], reflecting the decrease of the X-ray absorption coefficient as a function of X-ray energy. It is seen that the positive slope of the electron-yield spectrum is clearly not representative of the true X-ray absorption coefficients. Its influence must therefore be corrected for during background subtraction and/or data analysis. To a good first approximation, this can be done by adjusting the pre-edge background function with a 'steering point' at the end of the spectrum. This is the approach which was adopted throughout the present work.

Representative pre-edge background functions have been plotted together with the raw EXAFS data in figs. 1.3. and 1.4. Subtraction of these pre-edge functions produces the normalised absorption spectra given in fig. 1.5. It is obvious that the curved, extrapolated pre-edge background in fig. 1.3. does not fully compensate for the artificially increased total electron-yield background function. Particularly at energies high above the absorption edge, the post-edge background is typically between 10% and 20% higher than the background function in the transmission spectrum. The deviations between the data sets are much smaller in the vicinity of the absorption edge and for photoelectron energies in the region below 200 eV (corresponding to a maximum k of approximately 7.25 \AA^{-1}). Because of these differences, subtraction of the post-edge background functions is expected to lead to

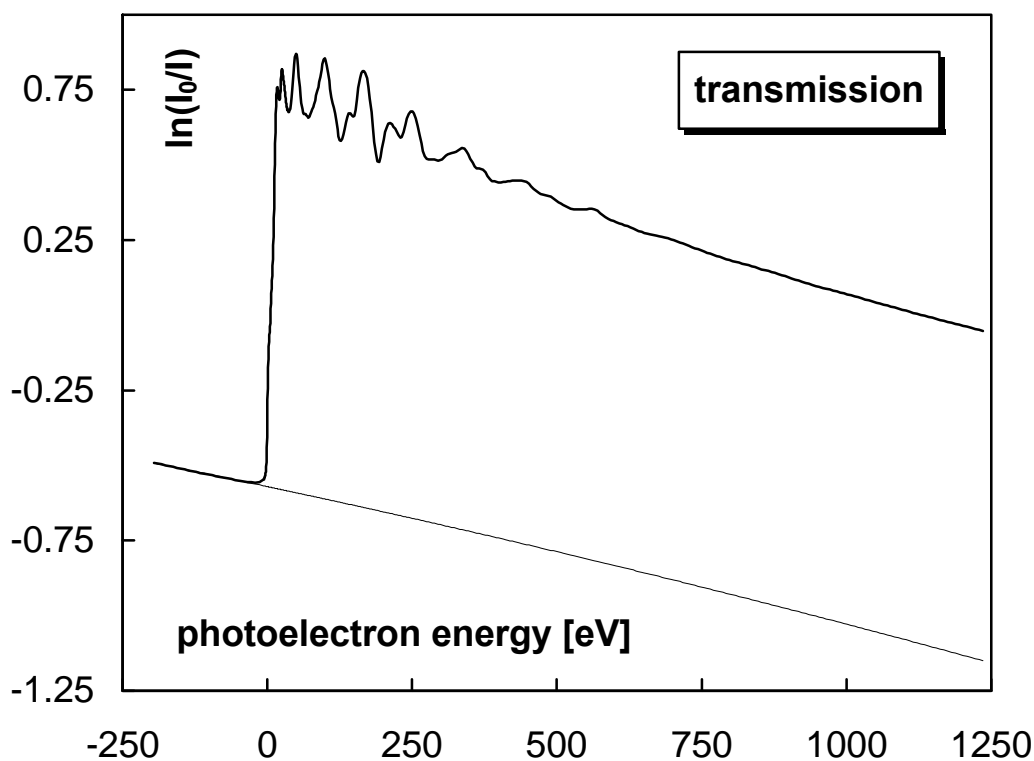


Figure 1.4. Transmission spectrum of a polycrystalline Ni foil (thickness: $10 \mu\text{m}$) with fitted 2nd-order polynomial pre-edge background function.

artificially reduced electron-yield EXAFS amplitudes, particularly at high k -values. However, examination of the post-edge background subtraction results reveals that the deviations between the extracted EXAFS functions are actually much smaller than the cursory inspection of fig. 1.5. suggests. The electron-yield EXAFS function does in fact exhibit an almost *uniform* amplitude reduction of the order of 5% - 10% of the transmission amplitude, rather than a k -dependent amplitude damping. The uniform amplitude reduction is very clearly seen even at $k < 6 \text{ \AA}^{-1}$. As will be discussed in more detail in chapter 4, its observation and the absence of an artificially damped amplitude can be rationalised in terms of a combination of the following effects:

1. The total electron-yield contributions from the X-ray induced primary K-shell photoelectrons become larger towards higher X-ray energies, as the kinetic energy of the photoelectrons, and thus their escape depth, increases. The photoelectron current carries EXAFS information, so that its increasing contribution to the absorption spectrum results in an enhancement of the EXAFS amplitude in the high k -range. This additional EXAFS contribution compensates in the data analysis for the upwards sloping background function. Note that this interpretation is at variance with the conclusions of Stöhr *et al.* [79] who argued that ‘only few’ of the emitted photoelectrons ‘will carry EXAFS information since the energy-loss processes [along the photoelectron trajectory from its origin to the surface] are likely to interfere with the [back-] scattering event [which is

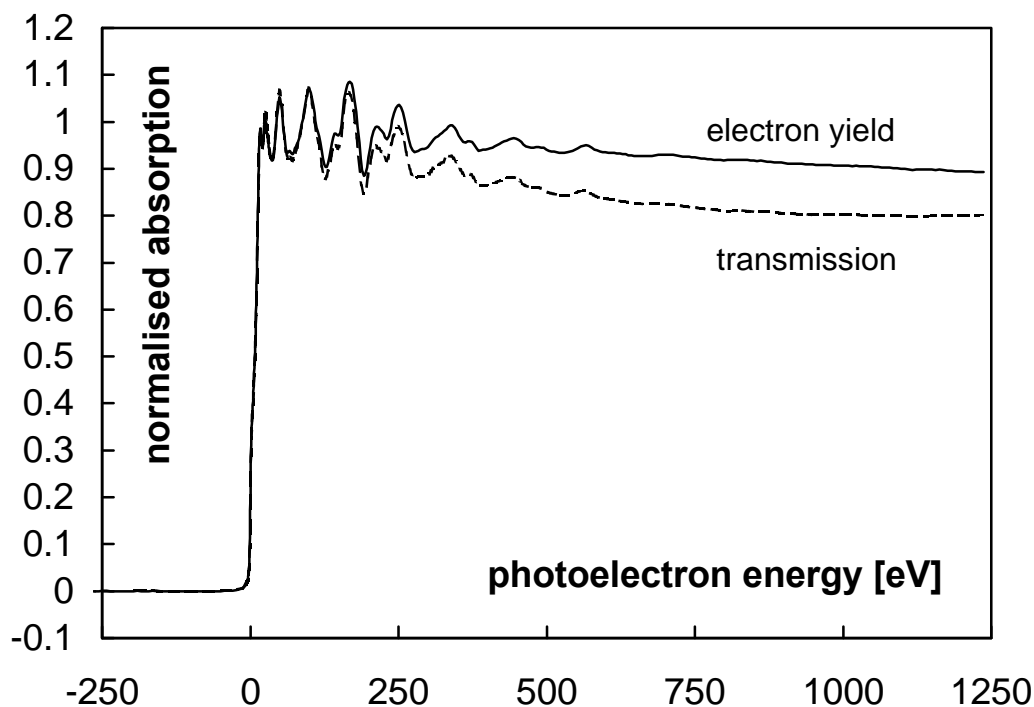


Figure 1.5. Pre-edge background subtracted spectra from figs. 3 and 4 normalised to the edge-step height. Note the different post-edge background functions.

responsible for the EXAFS]'. It appears that Stöhr *et al.* have overlooked that the majority of the photoelectrons *do* finally escape from the local environment of the X-ray excited atoms. They seem to confuse extrinsic and intrinsic EXAFS amplitude losses due to many-body effects with the inelastic losses which merely limit the sample penetration by the photoelectrons that have escaped from the vicinity of the photoexcited atomic core. These latter losses should not influence the initially formed core hole, as they affect electrons which are not involved in the modification of the final state of the photoexcited atom.

2. The overall reduced EXAFS amplitude is due to total electron-yield contributions excited by self absorbed fluorescence photons. Because of the well-known 'self-absorption' effect [17, 21-24] the fluorescence-yield signal yields strongly reduced EXAFS amplitudes.
3. The formation of a thin oxide layer on the surface of the Ni samples, evident in the electron-yield spectrum as a small near-edge feature (indicated by the arrow in fig. 1.3.) characteristic of NiO, might also reduce the observed EXAFS amplitude somewhat. Closer examination of the intensity of this near-edge feature reveals that it represents oxide fractions of less than 2% of the electron-yield signal (compare to the strong intensity of this feature in spectra of NiO given in chapters 3 and 6). Its influence is therefore of minor importance.
4. The transmission of the ionisation chamber used as the monitor for the intensity

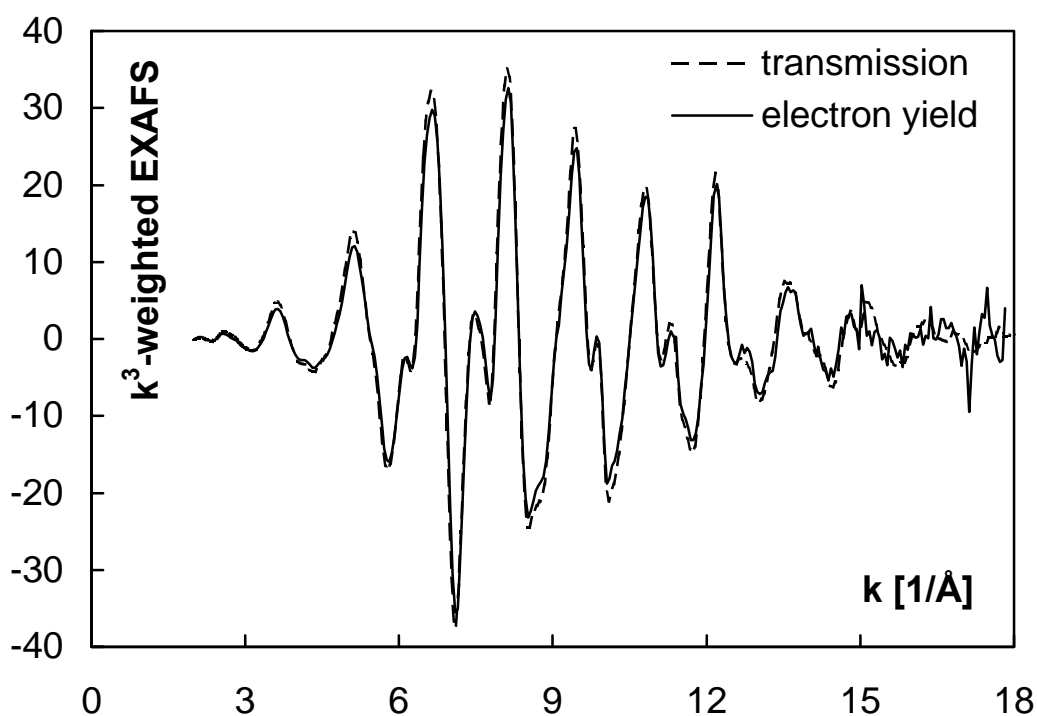


Figure 1.6. k^3 -weighted EXAFS functions obtained from the normalised spectra in fig. 1.5.

of the incoming beam and the air paths between ionisation chamber and sample increase with photon energy. As a result, the beam intensity at the sample is approximately 10% higher at the end of a long scan than at the absorption edge.

In summary, the error introduced into the EXAFS function during the post-edge fitting procedure is roughly comparable for electron-yield and transmission data of Ni metal. The analysis of total electron-yield and transmission data gives therefore similar results, provided that the extrapolation of the pre-edge background function takes account of the positive slope of the electron-yield background. By comparative examination of a wider range of electron-yield and transmission spectra (not presented in this thesis) it can be asserted that this conclusion is generally valid. To the author's knowledge this is the first time that the compensating influence of the photoelectron EXAFS at higher energies has actually been identified in experimental data.

1.5. EXAFS Data Analysis

The analysis of all EXAFS data in the present work employed the code EXCURV92 [57] available at the EPSRC Daresbury Laboratory. In the present section, only a brief summary of the most important features of the EXAFS analysis procedure will be given. A thorough discussion of alternative EXAFS analysis techniques, as developed over the last decade, is beyond the scope of this introductory chapter, particularly since this area is still rapidly evolving. The interested reader will find many useful references to the most recent developments in the extensive proceedings of the 'XAFS' conferences held every two years*. For a recent comparison of alternative analysis techniques the reader is referred to the comparative study of Vaarkamp *et al.* [47].

Much information can usually be gained from an inspection of the Fourier transform of the EXAFS function. Before transforming, the experimental EXAFS is conventionally cut off at a carefully chosen k -value corresponding to several 10 eV (typically about 30 eV, $k \approx 2-3 \text{ \AA}^{-1}$) above the absorption edge. This cut-off is necessary because of the uncertainties about the true background function in the near-edge region. Calculation of the Fourier transform modulus of the experimental $c(k)$ function produces a real space spectrum which can be interpreted as a pseudo-radial distribution function (RDF) of the atoms around the absorber**. The positions of shell

* The proceedings of the last four conferences have been published in: *Physica B* **208&209** (1995), *Jpn.J.Appl.Phys. Suppl.* **32-2** (1993), *X-ray Absorption Fine Structure*, edited by G. Bunker *et al.* (Ellis-Horwood, New York, 1991), and *Physica B* **158** (1989).

** It is called a *pseudo*-RDF because of an offset of the radial axis due to the phase shifts experienced by the photoelectron wave (cf. section 1.1).

boundaries become visible as intercepts with the R-axis both in the absolute magnitude and the imaginary part of the Fourier transformed spectrum. In the early years of EXAFS studies, structural information was thus derived directly from the Fourier transform using model compounds and employing the concepts of phase shift and amplitude transferability [33,34,80-82]. Some authors still prefer this semi-empirical approach, extracting phase shifts and backscattering amplitudes from model compounds *via* Fourier filtering, rather than calculating all parameters from first principles [37,69,83-85]. This approach has the advantage that a single scattering expression as given by equation (1.6) can be employed in the data analysis, because all the curved-wave scattering parameters are correctly known from experiment.

The EXAFS analysis based on EXCURV92 involves fitting a fully theoretical EXAFS function based on the FCW expression derived by Gurman and co-workers [53,54]. The first step in this analysis is the setting up of a model lattice for the calculation of the atomic potentials needed for the determination of backscattering amplitudes and phase shifts. Currently, the best available method for the calculation of reliable potentials is the approach based on overlapping atomic scattering potentials using a Hedin-Lundqvist self-energy, until recently implemented only in the FEFF suite of *ab initio* codes [48-50,59-61]. The relevant calculations are possible also in EXCURV92, however, and this option was used throughout the present work. As the limitations of this method are unknown, it is highly recommended to test all calculated backscattering and phase shift functions against the EXAFS spectra of suitable model compounds of known structure. It is encouraging that this procedure did not yield indications of any severe problems throughout the analysis of data reported in this thesis. A slight indication of unreliable phase shifts became only apparent in the analysis of 3rd row transition metal data. Other workers have communicated similar problems with high-Z atoms [86-88].

The next step in the analysis is the refinement of the parameters in a structural model for the sample using the curved-wave theory. This is an iterative process based on statistical tests to characterise the goodness of the obtained fit [89-92]. In the present work, the goodness of fit will be reported in terms of 'R-factors' which can be rationalised in the following way [90]. The curve fitting procedure involves principally the minimisation of a normalised sum of squares of residuals Φ given by

$$\Phi = \sum_i \frac{1}{s_i^2} \cdot (\mathbf{c}_{expt}(k_i) - \mathbf{c}_{theor}(k_i))^2, \quad (1.14a)$$

where $c_{expt}(k_i)$ and $c_{theor}(k_i)$ are the experimental and theoretical EXAFS functions, respectively, while

$$\frac{1}{s_i} = \frac{k_i^n}{\sum_j k_j^n \cdot |c_{expt}(k_j)|} = \frac{k_i^n}{M}. \quad (1.14b)$$

is the normalisation factor which accounts for the k-weighting and M , the so-called amplitude term, which is a spectrum-specific constant introduced to allow comparison of the Φ -values for spectra of different overall amplitude. The R-factor is defined somewhat differently, as

$$R = \sum_i^N \frac{1}{s_i} \cdot \left(|c_{expt}(k_i) - c_{theor}(k_i)| \right) \cdot 100\%, \quad (1.15)$$

and likewise gives an indication of the quality of the k-weighted fit to the EXAFS function. Note that R and Φ do not necessarily assume a minimum value for the same set of fitting parameters. Their values should principally be taken as complementary information on the fit quality. Note also that the choice of a longer k-space window will in practice worsen the agreement with experimental data because of the larger scatter in the data at higher k values. Only fit factors of datasets analysed over the same k-window can therefore be compared directly. As a rule of thumb, R-factors around 20% are normally considered a good fit, while figures above 40% indicate poor correlation between theory and experiment [90,92].

Attention should also be paid to the choice of the value of the weighting parameter n during the data analysis. Values of 2 or 3 are often used to compensate for the decay of the EXAFS at high k-values and to generate a larger number oscillations with high amplitudes. What is often ignored is the fact that the emphasis on the high-energy part of the spectrum also enhances the EXAFS contributions of strong backscatterers (typically high-Z elements) at the expense of weak (low-Z) backscatterers [85]. The analysis of strongly k-weighted EXAFS becomes therefore unreasonably more sensitive to the high-Z contributions. This is a particular problem for the EXAFS analysis of compounds between 3rd row transition metals and low-Z elements. It is generally considered good practice to calculate the goodness of a chosen fit to the data at several k-weightings to identify problems introduced by the choice for k. Clearly, such comparisons require also that the data are noise-free over the investigated k-range.

The maximum number of statistically significant degrees of freedom, P , in the fitting procedure is determined by the available range of k - and R -space containing meaningful structural information [93]:

$$P = \frac{2 \cdot \Delta k \cdot \Delta R}{p} + 2 \quad (1.16)$$

This result, usually referred to as ‘Nyquist’s theorem’, is a rigorous requirement of information theory [93-96]. The constraints it imposes on the data analysis can be very restrictive. For example, the most pronounced R -contributions in first row transition metal data cover a Fourier R -window from approximately 2 Å to 5.5 Å. Assuming a spectrum of medium quality, with an available k -range of - typically - 3 Å to 12 Å, the number of degrees of freedom becomes approximately 23. Each fitted coordination shell requires the determination of 3 parameters (coordination number, Debye-Waller factor, distance to the absorber), while two degrees of freedom are consumed by fitting the threshold energy and the uniform amplitude loss parameter S_0 . This leaves only seven coordination shells which can be fitted to the data in a statistically meaningful fashion. For compounds, the extent of coordination shell information contained in the experimental data is thus quickly exhausted by , even for relatively simple structures.

Further considerations requiring attention have been summarised in the first *Report on the International Workshops on Standards and Criteria in XAFS* [71], amendments to which are published regularly in the proceedings of the international XAFS conferences held every two years (*vide supra*). This report does also give important recommendations about the publication of XAFS data.

1.5. References

- [1] D.M. Pease, *Appl. Spectrosc.* 30 (1976) 405.
- [2] W.W. Beeman, H. Friedman, *Phys. Rev.* 56 (1939) 392.
- [3] L.V. Azároff, B.N. Das, *Phys. Rev.* 134 (1964) A747.
- [4] R.A. van Nordstrand, *Adv. Catal.* 12 (1960) 149.
- [5] L.G. Parratt, C.F. Hempstead, E.L. Jossen, *Phys. Rev.* 105 (1957) 1228.
- [6] J.O. Porteus, *J. Appl. Phys.* 33 (1962) 700.
- [7] U. Landman, D.L. Adams, *Proc. Natl. Acad. Sci. U. S. A.* 73 (1976) 2550.
- [8] P.A. Lee, *Phys. Rev. B* 13 (1976) 5261.
- [9] W. Gudat, C. Kunz, *Phys. Stat. Solidi* 52 (1972) 433.
- [10] W. Gudat, C. Kunz, *Phys. Rev. Lett.* 29 (1972) 169.

- [11] J. Jaklevic, J.A. Kirby, M.P. Klein, A.S. Robertson, G.S. Brown, P. Eisenberger, *Solid State Commun.* 23 (1977) 679.
- [12] J. Stöhr, D. Denley, P. Perfetti, *Phys. Rev. B* 18 (1978) 4132.
- [13] P.H. Citrin, P. Eisenberger, R.C. Hewitt, *Phys. Rev. Lett.* 41 (1978) 309.
- [14] G. Martens, P. Rabe, N. Schwentner, A. Werner, *J. Phys. C* 11 (1978) 3125.
- [15] J. Stöhr, L.I. Johansson, I. Lindau, P. Pianetta, *Phys. Rev. B* 20 (1979) 664.
- [16] H. Petersen, C. Kunz, *Phys. Rev. Lett.* 35 (1975) 863.
- [17] J. Goulon, C. Goulon-Ginet, R. Cortes, J.M. Dubois, *J. Phys. (Paris)* 43 (1982) 539.
- [18] J. Stöhr, *NEXAFS Spectroscopy (Springer Series in Surface Sciences 25)* (Springer, Berlin, Heidelberg, 1992).
- [19] J. Stöhr, E.B. Kollin, D.A. Fischer, J.B. Hastings, F. Zaera, F. Sette, *Phys. Rev. Lett.* 55 (1985) 1468.
- [20] J.B. Hastings, *EXAFS of Dilute Systems: Fluorescence Detection*, in: *EXAFS Spectroscopy*, ed. by B.K. Teo and D.C. Joy (Plenum Press, New York, London, 1981) 171.
- [21] T.M. Hayes, J.B. Boyce, *Solid State Phys.* 37 (1982) 173.
- [22] L. Tröger, D. Arvanitis, K. Baberschke, H. Michaelis, U. Grimm, E. Zschech, *Phys. Rev. B* 46 (1992) 3283.
- [23] D.M. Pease, D.L. Brewster, Z. Tan, J.I. Budnick, C.C. Law, *Phys. Letters A* 138 (1989) 230.
- [24] Z. Tan, J.I. Budnick, S.M. Heald, *Rev. Sci. Instrum.* 60 (1989) 1021.
- [25] E.A. Stern, *Theory of EXAFS*, in: *X-Ray Absorption. Principles, Applications, Techniques of EXAFS, SEXAFS and XANES*, ed. by D.C. Koningsberger and R. Prins (John Wiley & Sons, New York, Chichester, Brisbane, Toronto, Singapore, 1988) 351.
- [26] M. Brown, R.E. Peierls, E.A. Stern, *Phys. Rev. B* 15 (1977) 738.
- [27] G. Mitchell, W.W. Beeman, *J. Chem. Phys.* 20 (1952) 1298.
- [28] Y. Cauchois, N.F. Mott, *Phil. Mag.* 40 (1949) 1260.
- [29] D.E. Sayers, F.W. Lytle, E.A. Stern, *Adv. X-ray Analysis* 13 (1970) 248.
- [30] D.E. Sayers, E.A. Stern, F.W. Lytle, *Phys. Rev. Lett.* 27 (1971) 1204.
- [31] F.W. Lytle, D.E. Sayers, E.B. Moore, *J. Appl. Phys.* 45 (1974) 45.
- [32] E.A. Stern, *Phys. Rev. B* 10 (1974) 3027.
- [33] F.W. Lytle, D.E. Sayers, E.A. Stern, *Phys. Rev. B* 11 (1975) 4825.
- [34] E.A. Stern, D.E. Sayers, F.W. Lytle, *Phys. Rev. B* 11 (1975) 4836.
- [35] A. Pinto, A.R. Pennisi, G. Faraci, G. Dagostino, S. Mobilio, F. Boscherini, *Phys. Rev. B* 51 (1995) 5315.

- [36] M. Vaarkamp, F.S. Modica, J.T. Miller, D.C. Koningsberger, *J. Catal.* 144 (1993) 611.
- [37] M. Vaarkamp, P. Dijkstra, J. van Grondelle, J.T. Miller, F.S. Modica, D.C. Koningsberger, R.A. van Santen, *J. Catal.* 151 (1995) 330.
- [38] S.J. Gurman, *J. Synchrotron Rad.* 2 (1995) 56.
- [39] J.J. Rehr, E.A. Stern, R.L. Martin, E.A. Davidson, *Phys. Rev. B* 17 (1978) 560.
- [40] T. Fujikawa, T. Miyanaga, *J. Phys. Soc. Jpn.* 62 (1993) 4108.
- [41] J.J. Boland, J.D. Baldeschwieler, *J. Chem. Phys.* 80 (1984) 3005.
- [42] J.J. Boland, J.D. Baldeschwieler, *J. Chem. Phys.* 81 (1984) 1145.
- [43] E. Sevillano, H. Meuth, J.J. Rehr, *Phys. Rev. B* 20 (1979) 4908.
- [44] G. Beni, P.M. Platzman, *Phys. Rev. B* 14 (1976) 1514.
- [45] P.W. Atkins, *Molecular Quantum Mechanics* (Cambridge University Press, Cambridge, U.K. 1983).
- [46] P.A. Lee, J.B. Pendry, *Phys. Rev. B* 11 (1975) 2795.
- [47] M. Vaarkamp, I. Dring, R.J. Oldman, E.A. Stern, D.C. Koningsberger, *Phys. Rev. B* 50 (1994) 7872.
- [48] S.I. Zabinsky, J.J. Rehr, A. Ankudinov, R.C. Albers, M.J. Eller, *Phys. Rev. B* 52 (1995) 2995.
- [49] J. Mustre de Leon, J.J. Rehr, S.I. Zabinsky, R.C. Albers, *Phys. Rev. B* 44 (1991) 4146.
- [50] J.J. Rehr, J. Mustre de Leon, S.I. Zabinsky, R.C. Albers, *J. Am. Chem. Soc.* 113 (1991) 5135.
- [51] T.E. Westre, A. DiCicco, A. Filipponi, C.R. Natoli, B. Hedman, E.I. Solomon, K.O. Hodgson, *J. Am. Chem. Soc.* 117 (1995) 1566.
- [52] T.E. Westre, A. DiCicco, A. Filipponi, C.R. Natoli, B. Hedman, E.I. Solomon, K.O. Hodgson, *J. Am. Chem. Soc.* 116 (1994) 6757.
- [53] S.J. Gurman, N. Binsted, I. Ross, *J. Phys. C* 19 (1986) 1845.
- [54] S.J. Gurman, N. Binsted, I. Ross, *J. Phys. C* 17 (1984) 143.
- [55] M. Newville, *Local Thermodynamic Measurements of Dilute Binary Alloys Using XAFS* (University of Washington, 1995). A postscript file of this thesis is available at: <http://krazy.phys.washington.edu/~matt/thesis/thesis.tar.gz>
- [56] S.J. Gurman, *J. Phys. C* 21 (1988) 3699.
- [57] N. Binsted, J.W. Campbell, S.J. Gurman, P.C. Stephenson, *SERC Daresbury Laboratory EXCURV92 Program* (1991).
- [58] B. Lengeler, *X-Ray Absorption and Reflection in the Hard-X-Ray Range*, in: *Photoemission and Absorption Spectroscopy of Solids and Interfaces with Synchrotron radiation*, ed. by M. Campagna and R. Rosei (North-Holland, Amsterdam, Oxford, New York, Tokyo, 1990) 157.

- [59] J.J. Rehr, R.C. Albers, S.I. Zabinsky, *Phys. Rev. Lett.* 69 (1992) 3397.
- [60] P.J. Ellis, H.C. Freeman, *J. Synchrotron Rad.* 2 (1995) 190.
- [61] J.J. Rehr, *Jpn. J. Appl. Phys Suppl.* 32-2 (1993) 8.
- [62] P.A. Lee, G. Beni, *Phys. Rev. B* 15 (1977) 2862.
- [63] E.D. Crozier, J.J. Rehr, R. Ingalls, *Amorphous and Liquid Systems*, in: *X-ray Absorption: Principles, Applications, Techniques of EXAFS, SEXAFS and XANES*, ed. by D.C. Koningsberger and R. Prins (Wiley-Interscience, New York, 1988) 373.
- [64] N. Alberding, E.D. Crozier, *Phys. Rev. B* 27 (1983) 3374.
- [65] B.S. Clausen, H. Topsoe, L.B. Hansen, P. Stoltze, J.K. Norskov, *Catalysis Today* 21 (1994) 49.
- [66] B.S. Clausen, H. Topsoe, L.B. Hansen, P. Stoltze, J.K. Norskov, *Jpn. J. Appl. Phys* 32 (1993) 95.
- [67] M. Bader, A. Puschmann, G. Ocal, G. Haase, *Phys. Rev. Lett.* 57 (1986) 3273.
- [68] P. Roubin, D. Chadesris, G. Rossi, J. Lecante, M.-C. Desjonquères, G. Tréglia, *Phys. Rev. Lett.* 56 (1986) 1272.
- [69] D.E. Sayers, B.A. Bunker, *Data Analysis*, in: *X-ray Absorption. Principles, Applications, Techniques of EXAFS, SEXAFS and XANES (Chemical Analysis, Vol. 92)*, ed. by D.C. Koningsberger and R. Prins (Wiley, New York, 1988) 211.
- [70] B.K. Teo, *EXAFS: Basic Principles and Data Analysis* (Springer Verlag, Berlin, Heidelberg, New York, Tokyo, 1986).
- [71] *Report on the International Workshops on Standards and Criteria in XAFS*, in: *X-ray Absorption Fine Structure*, ed. by G. Bunker, S.S. Hasnain and D.E. Sayers (Ellis-Horwood, New York, London, etc. 1991) 751.
- [72] J.W. Cook, D.E. Sayers, *J. Appl. Phys.* 52 (1981) 5024.
- [73] M. Newville, P. Livins, Y. Yacoby, J.J. Rehr, E.A. Stern, *Jpn. J. Appl. Phys* 32-2 (1993) 125.
- [74] N. Binsted, University of Southampton (1989)
- [75] C.H. Reinsch, *Numer. Math.* 10 (1967) 177.
- [76] J.A. Victoreen, *J. Appl. Phys.* 19 (1948) 855.
- [77] J.A. Victoreen, *J. Appl. Phys.* 20 (1949) 1141.
- [78] J.A. Victoreen, *J. Appl. Phys.* 14 (1943) 95.
- [79] J. Stöhr, C. Noguera, T. Kendelewicz, *Phys. Rev. B* 30 (1984) 5571.
- [80] K.I. Pandya, D.C. Koningsberger, *Physica B* 158 (1989) 386.
- [81] B. Lengeler, *J. Phys. (Paris)* 47 C8 (1986) 75.
- [82] E.A. Stern, B.A. Bunker, S.M. Heald, *Understanding the Causes of Non-Transferability of EXAFS Amplitude*, in: *EXAFS Spectroscopy*, ed. by B.K. Teo and D.C. Joy (Plenum Press, New York, London, 1981) 59.

- [83] J.B.A.D. van Zon, D.C. Koningsberger, H.F.J. van't Blik, D.E. Sayers, *J. Chem. Phys.* 82 (1985) 5742.
- [84] M. Vaarkamp, J.T. Miller, F.S. Modica, G.S. Lane, D.C. Koningsberger, *J. Catal.* 138 (1992) 675.
- [85] M. Weissmüller, *J. Mater. Res.* 9 (1994) 4.
- [86] A.F. Lee, personal communication (1995)
- [87] P. Meehan, personal communication (1995)
- [88] J.W. Couves, personal communication (1995)
- [89] N. Binsted, R.W. Strange, S.S. Hasnain, *Jpn. J. Appl. Phys.* 32-2 (1993) 141.
- [90] N. Binsted, R.W. Strange, S.S. Hasnain, *Biochemistry* 31 (1992) 12117.
- [91] R.W. Joyner, K.J. Martin, P. Meehan, *J. Phys. C* 20 (1987) 4005.
- [92] N. Binsted, S.L. Cook, J. Evans, G.N. Greaves, R.J. Price, *J. Am. Chem. Soc.* 109 (1987) 3669.
- [93] E.A. Stern, *Phys. Rev. B* 48 (1993) 9825.
- [94] P.A. Lee, P.H. Citrin, P. Eisenberger, B.M. Kincaid, *Rev. Mod. Phys.* 53 (1981) 769.
- [95] E.O. Brigham, *The Fast Fourier Transform* (Prentice-Hall, Inc. Englewood Cliffs, New Jersey, 1974).
- [96] L. Brillouin, *Science and Information Theory* (Academic Press, New York, 1962).